NASA TECHNICAL MEMORANDUM NASA TM 75564

WORKING MODEL OF THE ATMOSPHERE AND NEAR PLANETARY SPACE OF JUPITER

V.I. Moroz, ed.

Translation of "Rabochaya Model' atmosfery i Okoloplanetnogo Prostranstva Yupitera," Academy of Sciences USSR, Insititute of Space Research, Moscow, Report PR-282, 1976, pp. 1-52.

(NASA-TM-75564) WORKING MODEL OF THE ATMOSPHERE AND NEAR PLANETARY SPACE OF JUPITER (National Aeronautics and Space Administration) 58 p HC A04/MF A01 CSCL 03B

N79-10984

Unclas
G3/91 33902

NATIONAL AERONAUTICS AND SPACE ADMINISTRATION
WASHINGTON, D.C. 20546 OCTOBER 1978

STANDARD TITLE PAGE

1. Report No.	2 Government Accession No	3 Recipient's Catalog No
NASA TM 75564		

4 Title and Subtitle	5 Report Date
WORKING MODEL OF THE ATMOSPHERE AND NEAR PLANETARY SPACE OF JUPITER	October 1978
	6 Performing Organization Code
7. Author(s)	8. Performing Organization Report No
V.I. Moroz, ed.	
	10 Work Unit No
9 Performing Organization Name and Address	11 Contract or Grant No
Leo Kanner Associates Redwood City, California 94063	NASW-3199
	13 Type of Report and Period Covered
12 Sponsoring Agency Name and Address	Translation
National Aeronautics and Space Administration, Washington, D.C. 20546	14 Sponsoring Agency Code

15 Supplementary Notes

Translation of "Rabochaya Model' atmosfery i Okoloplanetnogo Prostranstva Yupitera," Academy of Sciences USSR, Institute of Space Research, Moscow, Report PR-282, 1976, pp. 1-52.

16 Abstract Basic physical characteristics of Jupiter, its gravitational field, atmosphere, electromagnetic radiation, magnetosphere, meteorite situation and satellites are presented in numerous tables, graphs and figures and discussed. Means of observation of the atmosphere and three models of the atmosphere are presented and analyzed.

17. Key Words (Selected by Author(s))	18. Distribution Statement
	Unclassified-Unlimited

19 Security Classif. (of this report)	20. Security Classif. (of this page)	21. No. of Pages	22. Price
Unclassified	Unclassified		

FOREWORD

Jupiter, the largest planet of the solar system, differs sharply from the Earth and terrestrial group of planets in many basic characteristics (mass, rotation, composition, atmospheric and deep interior structure, etc.). Until recently, Jupiter had been studied only by means of ground based telescope astronomy. The flights of Pioneer-10 and Pioneer-11 demonstrated the possibility of the use of space vehicles for this purpose, despite the high level of hard radiation near the planet.

The proposed model summarizes the basic data on structure of the atmosphere and near planetary space of Jupiter, published by the beginning of 1976. In approach to the problem and structure, the work is similar to the models of the atmospheres of Venus and Mars, previously compiled at the Institute of Space Research, Academy of Sciences USSR [1,2]. Several possible alternate versions of the vertical profile of the atmosphere, selected so as to obtain a "bracket" of the basic parameters (temperature and pressure) over a wide range of altitudes, are given. In distinction from the previously published models of the terrestrial group of planets, considerable attention was given to the physical conditions in the near planetary space (radiation and meteorite situation). The model was compiled by the following group of authors: V.I. Moroz (basic characteristics, model of the atmosphere, electromagnetic radiation, meteorite situation, satellites), P.Ye. El'yasberg (gravitational field and satellites), M.N. Izakov and V.S. Zhegulev (model of the atmosphere), G.A. Skuridin, Yu.I. Gal'perin and K.I. Gringayz (magnetosphere and radiation situation).

TABLE OF CONTENTS

WORKING MODEL OF THE ATMOSPHERE AND NEAR PLANETARY SPACE OF JUPITER

V.I. Moroz, ed.
Institute of Space Research,
Academy of Sciences USSR, Moscow

1. Basic Physical Characteristics and Gravitational Field

1.1. Planetary Motion

Jupiter rotates about the sun in an elliptical orbit, with a semimajor axis of 5.203 AU and eccentricity 0.0484. The rectangular geoequatorial, heliocentric coordinates and velocity components are presented in [3]. The maximum error of each coordinate of Jupiter corresponding to these data can be assumed to be $3 \cdot 10^{-6}$ AU and, of each velocity component, $3 \cdot 10^{-9}$ AU/day [4]. /4*

1.2. Dimensions and Shape

The shape of Jupiter is described by an ellipsoid of rotation. The equatorial radius, polar radius and compression are presented in Table 1. The recommended value of the equatorial radius is based on the results of radiooccultation of the atmosphere of Jupiter by Pioneer-10 and Pioneer-11 [5], and it is relative to the 1 atm equipotential level. The value presented in work [5] for the 0.16 atm level was extrapolated downward, by means of the models of the atmosphere presented in section 2.2. The indicated error of ±30 km includes both measurement errors and indeterminancy in the models of the atmosphere.

The recommended value of the compression was determined as a result of analysis of the Pioneer-10 orbital data [6] and, within

*Numbers in the margin indicate pagination in the foreign text.

the limits of error, it coincides with the value found from the motion of the satellites [7], as well as with the geometric compression, obtained by means of micrometric measurements [8].

The radius of the planet at latitude ϕ is connected with the equatorial radius by the relation

$$R_\varphi = R_e (1 - \varepsilon \sin^2 \varphi). \quad (1)$$

The values of R_ϕ for various latitudes are presented in Table 2.

1.3. Mass and Gravitational Field

In expansion of potential V of the gravitational field of Jupiter by Legendre polynomials, it is sufficient to leave three terms: /5

$$V(r, \varphi) = \frac{\mu}{r}\left[1 - I_2 \left(\frac{R_e}{r}\right)^2 P_2(\sin\varphi) - I_4 \left(\frac{R_e}{r}\right)^4 P_4(\sin\varphi)\right], \quad (2)$$

where μ is the gravitational parameter, I_2 and I_4 are the coefficients of the harmonics, R_e is the equatorial radius.

There now are several determinations of the mass of Jupiter from observations of the satellites of Jupiter, small planets and from orbital measurements of space probes (Pioneer-10,11) [6].

In accordance with the recommendations of the International Astronomical Union (IAU), the ratio of the mass of the sun to the mass of Jupiter should be assumed to be 1047.355 with a maximum error ± 0.025, and the gravitational parameter of the

sun (132712438000 ± 5000)km^3/sec^2. From this, for the gravitational parameter of Jupiter, we obtain

$$\mu = (126712000 \pm 3000)\ \text{km}^3 \cdot \text{sec}^{-2}$$

For the remaining constants in formula (2), the following values, determined by Anderson et al [6], can be assumed:

$$\begin{aligned} \bar{I}_2 &= (1.4720 \pm 0.0040) \cdot 10^{-2}, \\ I_4 &= (-650 \pm 150) \cdot 10^{-6}, \\ R_e &= 71398\ \text{km}. \end{aligned} \qquad (3)$$

The value of R_e obtained by Anderson differs somewhat from that recommended above (and subsequently used for models of the atmosphere).

The acceleration of gravity depends appreciably on latitude. Centrifugal force makes a significant contribution. The acceleration of gravity for different latitudes is presented in Table 2. For calculations of models of the atmosphere, we will assume

$$g = 25\ \text{m/sec}^2. \qquad (4)$$

The change of g with altitude can be disregarded in these calculations.

1.4. Rotation

The observable details on the disc of the planet belong to the cloud layer. However, there are compact and long lasting formations (spots) among them, from which the period of rotation can be determined. Since atmospheric motions, the velocity of which is somewhat different at different latitudes, make a

/6

contribution to the observable rotation effect, the average period determined from the movement of details depends somewhat on latitude. It has been determined that, near the equator (±12°), the spots have a period of rotation of 9 hours 50 min, but it is close to 9 hours 55 min in the middle latitudes. The periodicity of change in intensity of radio emissions in the decimeter range and the frequency of bursts in the decameter range (see section 3) are close to the period of rotation in the middle latitudes; however, they are not completely consistent.

In connection with this, three systems of longitude are used to designate the coordinates on Jupiter: system I (equatorial), II (for middle latitudes) and III (for radio emission). The corresponding periods are given in Table 3. The zero meridians for these systems were selected arbitrarily, and they are not connected with any definite details. At a time in 1897, July 14.00, Julian day 2414120.0, the central meridian of the planet had a longitude of 43.31° in system I and 96.58° in system II [9]. The zero meridions in systems III and II coincided on 1 January 1957, at zero hours UT [10]. Since there evidently is no solid core in Jupiter, and the thickness of the gaseous atmosphere is over 1000 km in any case (see section 2), the rotation rate probably depends on both latitude and depth. The basic mass of Jupiter, which is in the liquid state, evidently has a period of rotation which corresponds to system III. The magnetosphere and radiation belts rotate with the same period.

The linear velocity of rotation at the equator is presented in Table 3. It exceeds the escape velocity on the Earth. The centrifugal acceleration is about 10% of the gravitational. /7

The inclination of the equator to the orbital plane is 3° 07'.

Because of the small inclination, there are no change of season phenomena on Jupiter.

2. Atmosphere

2.1. Chemical Composition

Spectroscopic observations of Jupiter long ago permitted the detection of hydrogen [11], methane and ammonia [12] in the atmosphere of the planet. Summaries of observational determination of these gases can be found in books [13,14]. Helium [15], acetylene [16], ethane [16], water vapor [17] and phosphine [18] have been added to them in recent years. Absolute determinations of the abundance of various gases in the atmosphere of Jupiter encounter considerable difficulty, because of the fact that the absorption lines form in a cloud medium with poorly known properties. In a number of cases, even relative determinations prove to be difficult. Helium in the lower atmosphere cannot be determined at all by direct spectroscopy, because of the absence of absorption lines. Its abundance can be estimated, only from the effect of other gases on the lines and from the luminoscity in the high layers of the atmosphere.

Nevertheless, analysis of observational data, including theoretical calculations of the internal structure, permit the highly likely hypothesis to be offered, that the elementary composition of the atmosphere and interior of Jupiter corresponds to the average cosmic abundances [13,14,19]. Consequently, the basic chemical components are hydrogen and helium.

In distinction from the terrestrial group of planets, the basic mass of matter of Jupiter evidently is not in the solid, but in the liquid state [20,21]. It is highly likely that such

elements as oxygen, carbon and nitrogen are uniformily mixed with hydrogen and helium, due to convection in the gas and liquid shells. All these considerations give a basis for adopting the following model of the chemical composition of the atmosphere for subsequent calculations. The basic components are molecular hydrogen and helium, in a ratio which corresponds to the average cosmic abundances (90% hydrogen atoms and 10% helium atoms, according to [22]). Oxygen, carbon and nitrogen are bound primarily in H_2O, CH_4 and NH_3 molecules, and their content is proportional to the average cosmic abundance of O, C and H. A model of the chemical composition of the atmosphere of Jupiter constructed in this manner is presented in Table 4. It is in satisfactory agreement with known spectroscopic estimates. The measured C_2H_6:CH_4 and C_2H_2:CH_4 ratios were used directly for ethane and acetylene. For H_2O and NH_3, the composition model is suitable, only below the corresponding condensation levels, the location of which depends on the vertical structure and which is noted in Fig. 1. Observation and theory do not completely exclude an increased (compared with the average cosmic distribution) helium content in the atmosphere of Jupiter. The maximum permissible He:H_2 bulk ratios evidently do not exceed 1. This ratio was adopted in section 2.2, for calculation of one alternate version of the vertical structure model (model II).

/8

2.2. Vertical Structure of Atmosphere

In distinction from the terrestrial group of planets, the main bulk of the matter of Jupiter does not differ in chemical composition from the atmosphere. The lower boundary of the atmosphere is determined by the phase transition of hydrogen to a degenerate (metallic) state, which evidently is liquid. This

transition occurs at a depth of about 15000 km [20,21,23]. The internal heat flux (comparable in magnitude to the flux obtained from the sun on the surface of the planet) produces high temperatures in the interior of Jupiter, and the mixture is in a supercritical state throughout, above the hydrogen-helium interface. /9

Observational data on the vertical structure of the atmosphere of Jupiter can be divided into several groups:

1. Determination of the rotational temperature and pressure from the width of the CH_4 and NH_3 spectral lines. They give values in the range of 150-250 K and 0.5-2 atm (see, for example, [12,13,24]). This level corresponds to the visible surface of the clouds.

2. Spectrophotometry of the thermal emission in the infrared range (λ>5 μm). It shows that the temperature is close to 180° at the 1 atm level, increases downward and decreases upward; at the 0.1-0.2 atm level, there is a minimum (115-120°) and, then, the temperature increases with increase in altitude [25-28]. At wavelengths around 5 μm, where the atmosphere of Jupiter is relatively transparent, brightness temperatures up to 300 K are observed in isolated places, which indicates an increase of temperature at great depths [29]. The wavelength averaged thermal emission rate of the planet is characterized by an effective temperature of around 130 K.

3. Thermal radio emission spectrum. Analysis of the spectrum in the 1.25 cm NH_3 line region gives T≈130 K at the 0.5 atm level [30]. The thermal component of the brightness temperature in the 3-10 cm range evidently increases to several hundred degrees. This indicates an increase in temperature at greater depths (see Section 3.3).

4. Photometric observations of star occultation by Jupiter [31-35]. They show that, at the $P \approx 10^{-6}$ atm level, the temperature is in the range from 140 to 220 K. There probably is an increase in temperature with decrease in altitude below this level.

5. Pioneer-10 and 11 radio occultation observations. These /10
measurements gave a tempeature of several hundred degrees at the 1 atm level, which sharply contradicts the group 1-3 data. The atmospheric profile at the 0.1 atm level basically is not consistent with the infrared spectrum. All this group of results are in great doubt. Part of the disagreements may be removed, by means of allowance for compression [36], which was not done in the initial processing program. It is not excluded that horizontal inhomogeneities in the atmosphere of Jupiter greatly reduce the reliability of the method. Below, we will be forced to disregard the radio occultation results in part of the structure of the lower atmosphere. However, radio occultation has provided qualitatively new information on the ionosphere and upper atmosphere of the planet [38,39]. Above the 10^{-6} atm level, the temperature increases with increase in altitude, and it probably reaches an asymptote with a value on the order of 700-800 K. This is significantly higher than in previously proposed models [40,41]. The principal electron concentration maximum ($n_e \approx 10^5 cm^{-3}$) occurs at an altitude of about 1000 km. There are several secondary maxima. At an altitude of 3000 km, the electron concentration decreases by an order of magnitude.

There are theoretical calculations of the vertical profile of the atmosphere of Jupiter, in the range from several atmospheres to $\sim$1 mb, which take account of the absorption of infrared radiation in the H_2 and NH_3 bands, solar radiation in the

CH_4 bands and, also, convection in the lower layers [26,27,37]. They give better agreement with the observational data of groups 1-3. It seems likely that, below the 1 atm level, there is an adiabatic gradient at all depths. However, detailed calculations, which take account of the change in opacity with depth, apparently have not been carried out.

The basic parameters of three models of the vertical structure of the atmosphere we have proposed are given in Table 5. They take into account the data listed above and their scatter. /11
T(P) curves for these models are presented in Fig. 1. Model I (average or basic) gives the most likely variation of the parameters with altitude. Model II (temperature minimum) gives an upper limit of density in the lower atmosphere and a lower limit in the high layers. Model III (temperature maximum) gives a lower limit of density in the lower atmosphere and an upper boundary in the high layers. The average molecular weight in models I and III $\mu=2.28$ and $\mu=3.00$ in model II. Below the P=1 atm level, a dry adiabatic gradient was used in models I and III. A gradient equal to half the dry adiabatic with the corresponding composition was used in model II.

The H_2O and NH_3 condensation levels are noted in Fig. 1. Ammonia and water clouds are located above these levels. Nevertheless, the adopted atmospheric composition permits the effect of the heat of condensation on temperature to be disregarded in the first approximation, since the concentration of the condensing components is rather small.

Vertical profiles of the atmosphere are presented in Tables 6-8 and Figs. 2 and 3, for the three models listed (temperature, pressure and density vs. altitude). P vs altitude was calculated from given P(T) profiles, by means of the barometric formula

$$P_2 = P_1 \exp\left\{-\int_{z_1}^{z_2} dz/H\right\}, \tag{5}$$

where P_1 and P_2 are the pressures at the boundaries of some layer of the atmosphere with altitudes Z_1 and Z_2,

$$H = \frac{RT(z)}{g}, \tag{6}$$

R is the gas constant.

In the intervals where T(P)=const (isothermal sections), formula (4) is reduced to the form

$$P = P_0 \exp\{-z/H\}, \tag{7}$$

in the intervals where T(Z) changes with altitude, the nonlinear approximation /12

$$T = T_0(1 + az), \tag{8}$$

is used, where

$$a = \frac{dT}{dz}$$

it is the temperature gradient, and formula (4) is reduced to the form

$$P = P_0 \left(\frac{T}{T_0}\right)^{\varkappa}, \tag{9}$$

where the polytropic exponent

$$\varkappa = \frac{g}{R \cdot dT/dz}. \tag{10}$$

In this case, if the atmosphere is in an adiabatic state,

$$\frac{dT}{dz} = -\frac{g}{c_p}; \tag{11}$$

$$\varkappa = \frac{c_p}{R} \tag{12}$$

The heat capacity values were taken from handbook [42]. The dependence of the H_2 heat capacity on temperature was taken into consideration.

It was assumed that the turbopause was located at an altitude where the numerical concentration $n=3\cdot10^{13}$ cm^{-3} ($P\approx10^{-6}$ atm). This corresponds to a turbulent mixing coefficient $D_T=10^6$ cm$^2\cdot$sec^{-1} (according to [32], $D_T=5\cdot10^5$cm$^2\cdot$sec^{-1}). In a layer approximately 100 km thick above the turbopause, the helium content becomes negligibly small with increase in altitude, and the average molecular weight above $\bar{\mu}=2$. The degree of dissociation of molecular hydrogen is assumed to be negligibly small at all altitudes.

2.3. Clouds and Winds

The highest directly observable story of clouds in the atmosphere of Jupiter evidently forms, due to the condensation of NH_3 (above the 0.6 atm level in model I). A story of H_2O clouds should be located below (above the 4 atm level in model I). It is proposed [43] that there may also be clouds of a water solution of NH_3 and solid NH_4SH particles in the atmosphere of Jupiter. A diagram of the altitude distribution of clouds of various natures, calculated for chemical composition models which differ little from that used in the present work, is presented in Fig. 4. /13

To explain the red color of the upper story of clouds, it must be assumed that, besides NH_3 crystals (transparent in the visible region of the spectrum), there is some coloring impurity in them. A large number of hypotheses has been proposed, to explain the cloud color (see [14]), but it is not possible to

assign a serious preference to a single one. One recent hypothesis explains the cloud color by a phosphorus particle impurity [44].

Dark reddish bands (sometimes called belts) cross the disc of Jupiter. The light intervals between the bands are called zones. The bands and zones extend along the parallels, which is explained by the predominantly zonal wind direction in the atmosphere.

The general pattern of the distribution of the bands and zones, their type and contrast and fine structure change over time. The primary details and their nomenclature are shown in Fig. 5. The light equatorial zone (E.Z.) extends along the equator. A fine narrow dark band sometimes is noticeable in the middle of it. Dark bands are located on both sides of the Equatorial Zone: South (S.E.B.) and North (N.E.B.) Equatorial. The South Equatorial Band consists of two components, as a rule. The other bands also frequently are broken down into two components. The North Tropical Zone (N.Trop.Z.) is located north of the N.E.B., the North Temperate Band (N.T.B.) beyond it and still further north, the N.N.T.B., N.N.N.T.B., etc. bands sometimes are distinguished. The intervals between them are called the N.N.T.Z., N.N.N.T.Z, etc. The contrast of the bands /14
and zones decreases with increase in latitude and, near 45°, th polar region begins, which has a more or less uniform color.

The bands and zones in the Southern Hemisphere form a similar structure; however, there are some characteristic features here. A dark oval object, the Great Red Spot, is located in the South Tropical Zone, and the southern edge of the S.E.B. bends around it, forming a "gulf." The red spot sometimes fades to total invisibility, but the gulf always remains noticeable.

The dimensions of the Great Red Spot are approximately 40000 x 15000 km.

The structure described is typical, but it is subject to changes in individual periods. There are "activity cycles," which are characterized by periodic changes in contrast, frequency of appearance of fast moving clouds and changes in location of the belts and zones.

The numerous atmospheric currents, which occupy more or less definite latitude intervals, are traced from the cloud movement. Velocity discontinuities at the edges of these currents reach 100 m/sec. The bands usually are located on the boundaries between the currents. An intense convection maximum evidently occurs here, and the upward transport of the coloring particles (phosphorous, for example,) occurs here more intensely; a dark band forms as a result. The Great Red Spot probably is a gigantic cyclone [45].

2.4 Electric Fields

Experimental data are lacking on the electric fields in the atmosphere of Jupiter. By analogy with the atmosphere of the Earth, the presence of separate sections, with intensities /15
up to $3 \cdot 10^4$ W/m, several kilometers in size for several hours, must be assumed in the troposphere (below the 0.2 atm level) [46]. The field intensity on a scale on the order of a few centimeters, for a few seconds before the occurence of lightning, can reach 10^6 W/m.

There is a hypothesis, according to which the formation of acetylene and ethane in the atmosphere of Jupiter is connected

with electrical discharges in the atmosphere [47]. In this case, the frequency of lightning reaches

$$N \simeq 5 \text{ km}^{-2} \cdot \text{Hour}^{-1}, \tag{13}$$

four orders of magnitude greater than on the earth.

3. Electromagnetic Radiation

3.1. Direct and Reflected Solar Radiation

The solar constant at the average distance of Jupiter from the sun (5.2 AU) is

$$Q = 51.0 \text{ W/m}^2. \tag{14}$$

Data on the monochromatic illumination E_λ produced by the sun at the same distance, the geometric albedo of Jupiter p_λ as a function of wavelength, and the average brightness of Jupiter B_λ at different wavelengths are presented in Table 9 [16,17]. The sharp fluctuations of a function in the $\lambda > 1$ μm region are caused by powerful CH_4, NH_3 and H_2 absorption bands. The average brightness was found from the formula

$$B_\lambda = \frac{E_\lambda p_\lambda \cos 45^\circ}{\pi}. \tag{15}$$

The reflectivity of the cloud layer of Jupiter obeys Lambert's law, in the first approximation. Typical contrast values of the dark and light formations in the cloud layer of Jupiter are presented in Table 10 [48].

3.2. Thermal Infrared Radiation

The effective infrared radiation temperature of Jupiter [13,14, 49] is /16

$$T_e = 128 \pm 5 \text{ K}. \tag{16}$$

It corresponds to the integral brightness of the thermal radiation of the planet

$$B = (4.8 \pm 0.8) \cdot 10^{-4} \text{ W} \cdot \text{cm}^{-2} \cdot \text{ster}^{-1}. \quad (17)$$

In the first approximation, T_e and B can be considered independent of latitude, longitude and time of day.

In a narrow wavelength section around 5 μm, the brightness temperature T_B reaches 200 and even 300 K in individual areas of the planet, the horizontal dimensions of which can exceed 10000 km [29].

3.3. Radio Emission

Radio emission of three types is observed: a. thermal; b. synchrotron; c. sporadic.

The thermal radio emission forms in the troposphere, and its intensity depends on its temperature and opacity. The brightness temperature of the troposphere is about 150 K in the 0.8-3 cm range, and it probably increases to 600 K at 10 cm. Beginning at 3 cm and at longer wavelengths, the synchrotron radiation intensity of the radiation belts becomes greater than the thermal radiation. The synchrotron radiation is the bremsstrahlung of high energy electrons captured in the magnetic field. The synchrotron radiation flux on the Earth can be considered independent of wavelength in the first approximation and equal to

$$F_\nu = 7 \cdot 10^{-26} \text{ W} \cdot \text{m}^{-2} \cdot \text{Hz}^{-1}. \quad (18)$$

The brightness temperature

$$T_B \approx 5 \cdot 10^3 \lambda^2,$$

where λ is the wavelength in meters. The synchrotron radiation intensity is almost constant over time. The radiation belts are /17

the source of the synchrotron radiation (Section 4.2). In calculation of T_B, it was assumed that the source is a 6 R_e diameter, 2 R_e thick disc.

At wavelengths of over 7.5 m, sporadic radio emission is predominant. It is a sequence of noise storms, which last from several minutes to several hours. They consist of short bursts, the duration of which varies from milliseconds to minutes, spectral width 0.5 mHz and total energy of up to $4 \cdot 10^9$ W·sec. The radiation is directional. The frequency of noise storms is on the order of one day (in observations from the Earth). The decameter emission evidently is generated, as a result of plasma oscillations in the ionosphere and plasma captured by the inner part of the radiation belts. The probability of the occurence of noise storms is different at different longitudes (minimum at 0-90° longitudes in longitude system III). There is a strong correlation of noise storm frequency with the orbital position of the Jupiter satellite Io.

4. Magnetosphere

Observations of the radio emission of Jupiter in the decimeter range more than 10 years ago showed that Jupiter has a strong magnetic field, in which high energy particles are trapped. The trapped high energy particles form radiation belts similar to those of the Earth, but much more powerful, both in geometrical dimensions, and in particle concentrations. Direct measurements of the magnetic field and charged particle fluxes in the vicinity of the planet were conducted by the Pioneer-10 and Pioneer-11 spacecraft. They basically confirmed radioastronomy results and /18
significantly refined them in detail. However, it should be noted that a single model of the magnetosphere of Jupiter, which takes critical account of both the radioastronomy and all available

direct measurements, has not yet been developed. Even on such a more or less narrow question as the results of direct magnetic field measurements, there are significant conflicts between different groups of investigators.

4.1. Magnetic Field

In the first approximation, the magnetic field of Jupiter (on the basis of analysis of both Pioneer-10 and Pioneer-11 data), can be represented as a simple dipole field, with moment $1.3 \cdot 10^{30}$ $G \cdot cm^3$, inclined to $10.5 \pm 0.6°$ at longitude $233 \pm 8°$ (system III) and shifted by 0.16 ± 0.09 R_e towards the point with latitude $9 \pm 8°$ and longitude $169 \pm 16°$. The magnetic moment of Jupiter is 4 orders of magnitude greater than the magnetic moment of the Earth. The field intensity at the magnetic equator (at the P=1 atm level) is

$$H \simeq 4 \text{ G}. \tag{19}$$

The quadrupole and octupole moments are 20 and 15%, respectively (which is somewhat greater than on the Earth). This model can be used out to a distance of approximately 10 R_e. For greater distances, the field of the magnetospheric currents and magnetopause currents must be taken into account and, for a more accurate calculation of the field at the surface of the planet and within 1-2 radii above it, the quadrupole and octupole terms, as well. A quantitative model of the magnetic field of Jupiter has been published, which contains 23 terms of expansion by spherical harmonics [50], which describe the measurements well, within 20 R_e.

At greater distances, the magnetic field of the electric c /19
currents in the magnetosphere and magnetopause, which are variable

and still inadequately determined, play a definite part. The qualitative pattern is that these currents cause a considerable increase in field intensity, so that the dimensions (radius) of the magnetosphere approximately double due to these currents, to ∿100 R_e, and the configuration of the currents, in the first approximation, corresponds to a thin ring around the axis of rotation of the planet, distorted by the "bumpiness" of the inclined magnetic dipole.

The magnetopause is a more or less spherical surface, with a radius on the order of 100 R_e, which easily changes this dimension, as a result of variations in the solar wind pressure. Fluctuations of tens of Jupiter radii are typical, and compression of the magnetopause to ∿50 R_e, i.e., by half, has been observed.

4.2. Magnetospheric Plasma

The proton component of the plasma in the 100 eV-4.8 keV energy range, has been recorded aboard Pioneer-10 in the magnetosphere of Jupiter, by means of electrostatic analyzers [51].

It turned out that four characteristic regions can be distinguished from the plasma data: "plasmasphere," inside the orbit of the Jovian satellite Io, at a distance of ∿6 R_e; "ring current," in the 8-15 R_e region, which is in the form of a plasma filled torus, which then is flattened to a thickness of 2 R_e in the equatorial plane and forms the "plasma layer"; between the plasmasphere and the ring current, there is a gap with radial dimensions ∿1-2 R_e, the proton "sporadic flux" zone. These four regions are characterized by the plasma parameters presented in Table 11. It should be noted that all

plasma measurements in the magnetosphere were carried out, against a background of strong hard radiation effects (see following section), they give rise to doubt, and they require further verification. /20

4.3. Energetic Particles in the Magnetosphere of Jupiter

From the point of view of the energetic particle distribution in it, the magnetosphere of Jupiter can be divided into three regions.

At 50-100 R_e, there is an energetic particle quasi-capture or diffusion region, or outer magnetosphere. Here, electron and proton fluxes of 10^2-10^4 $cm^{-2} \cdot sec^{-1}$ are recorded, with energies $E_e \sim 0.4$-1 MeV, $E_e > 6$ MeV and $E_p \sim 1.2$-2.15 MeV. Periodic variations of flux intensities are observed, with a period of 10 hours. The energy spectra have the form $E^{-\gamma}$, where $\gamma = 1.2$-2 for electrons and $\gamma = 4$ for protons [52].

At 25-50 R_e, the nature of the particle distribution changes. Here, the particles evidently begin to be entrained by the rapid rotation of the planet. The shape of the energy spectrum changes from power to exponential [53]. According to the data of [54], however, the proton spectrum has the form $E^{-\gamma}$, with $\gamma = 1.9$ in this region. The fluxes of protons with energies of 0.5-2.1 MeV and 1.2-2.1 MeV are $\sim 10^3$-10^4 $cm^{-2} \cdot sec^{-1}$ in this region and, of electrons with energies 0.1-2 MeV, 10^4 $cm^{-2} \cdot sec^{-1}$. Finally, there is an inner region in the magnetosphere, <20 R_e in size, in which stable particle capture by the magnetic field is observed, the 10 hour periodic variations in particle intensity are lacking, and the particle fluxes are 2-3 orders of magnitude greater than in other regions of the magnetosphere.

According to [54], the spectrum in the 13-25 R_e region has the form $E^{-\gamma}$, in which $\gamma=2.6$. The flux intensity does not depend on magnetic latitude, and the angular distribution is basically isotropic.

The characteristics of the energetic particles and their distribution in the inner region of the magnetosphere, at <20 R_e and in the core, at <6-8 R_e, are presented in Table 12 [52-57]. The flux distribution of electrons with energies of over 21 MeV, according to [55], are presented in Fig. 6. /21

It should be noted that the hard radiation intensity in the magnetosphere of Jupiter is 1.5-2 orders of magnitude greater than the fluxes of electrons and protons of the corresponding energies in the magnetosphere of the Earth, and that the extent of the radiation belts greatly exceeds the extent of the terrestrial radiation belts. The radiation level inside the magnetosphere of Jupiter is very high, especially in the region of the magnetic equator. Pioneer-10 received a radiation dose of about 500000 rad (1000 times more than the lethal human dose).

5. Meteorite Situation

Measurements of the meteorite concentrations near Jupiter and in the interplanetary space between the Earth and Jupiter were carried out by Pioneer-10 and 11 [58-61]. Models of the meteorite situation, constructed on the basis of analysis of these data, are presented in Table 13.

A region of increased meteorite concentration should be expected near Jupiter [62], the existence of which was confirmed for small particles ($\sim 10^{-5}$ cm), by direct measurements with the

use of micrometeorite sensors [58-61]. The zone of increased concentration evidently is a disc shaped region about $2 \cdot 10^7$ km in diameter and from 2 to $5 \cdot 10^6$ km thick (the planet in the center of the disc). Models of the meteorite situation beyond this region and inside it (zones A and B, respectively), are given separately in Table 13.

In the central portion of zone B, Pioneer-10 noted a two orders of magnitude increase in the impact rate (for 10^{-4}-10^{-3} cm and $\sim 10^{-9}$ g particles). This increase evidently is explained by a simultaneous increase in concentration and average encounter velocity. For zone B, the Table 13 data can be considered as only the very first, to the highest degree estimated approximation. They are of the least certain nature for large bodies (10^{-2} cm or more). Here, the spectrum has the same dimensions as in zone A, although experimental data are lacking. /22

The primary direction of movement in zone A is straight line (probably, at least 90% of the meteorites move in a straight line). In zone B, the fraction of meteorites in retrograde motion apparently is greater than in zone A.

6. Satellites

At the time the models were compiled, orbital data of 12 Jovian satellites were known. A report on the discovery of a thirteenth satellite has been received. A summary of the Jovian satellite orbits and dimensions is given in Table 14.

Four satellites, Io, Europe, Ganymede and Callisto, are close to the moon in size, and one of them (Io) undoubtedly has an atmosphere, and there is a great probability that Ganymede has one.

The values presented in Table 15 should be taken as the average orbital elements of the Jovian satellites at time T reckoned in days from 0.5 UT January, epoch 1950. They were taken from work [64]. The following designations were adopted in the Table:

i. angle of inclination of satellite orbit to orbital plane of Jupiter, epoch 1950.0;

$\hat{\omega}$. argument of the pericenter;

Ω. Longitude of the ascending node of the satellite orbit in the orbital plane of Jupiter, reckoned from the equatorial equinox of the earth to the ascending node of the orbit of Jupiter at the equator of the Earth and, then, in the orbital plane of Jupiter (the orbital plane of Jupiter, equator of the Earth and equinox of the Earth correspond to the 1950.0 epoch); λ is the mean longitudine of the satellite, equal to $\lambda = \Omega + \omega + v$, where v is the true anomaly. Besides the orbital elements, the value of gravitational parameter μ is given in Table 15. /2

Data on the physical characteristics of the four largest Jovian satellites are presented in Table 16.

References

1. Moroz, V.I., "Working Model of the Atmosphere of Venus," Institute of Space Research Preprint Pr-162, 1974.

2. Moroz, V.I. (ed), "Working Model of Atmosphere and Surface of Mars," Institute of Space Research Preprints Pr-240 and Pr-241, Moscow, 1975.

3. "Supplement to Astronomical Annual," Nos. 20-21, Leningrad, 1974.

4. Oesterwinter, Cl., and Ch.J. Cohen, Celestial Mechanics 5, 317 (1972).

5. Kliore, A., G. Fjeldbo and B.L. Seidel et al., Science 188, 474 (1975).

6. Anderson, J., G.W. Null and Wong, J.G.R. 79, 3661 (1974).

7. Brauer, D. and J.M. Clemens, Planety i sputniki [Planets and Satellites], G. Kuiper and B. Middlehurst (ed), Foreign Literature Publishing House, Moscow, 1963.

8. Dollfus, A., Icarus 12, 101 (1970).

9. Sharonov, V.V., Pripoda planet [The nature of the Planets], Fizmatgiz Press, 1957.

10. Galle, R.M., Planety i sputniki [Planets and Satellites] Foreign Literature Publishing House, Moscow, 1963.

11. Kiess, C.C., C.H. Corliss and H.R. Kiess, Astrophys. J. 132, 221 (1960).

12. Wildt, R., Veroff. Univ. Sternwarte Göttingen 22, (1932).

13. Moroz, V.I. Fizika planet [Physics of the Planets], Nauka Press, Moscow, 1967.

14. Teifel', V.G. (ed), Fizicheskiye kharakteristiki planet-gigantov [Physical Characteristics of the Jovian Planets], Nauka Kaz. SSR Press, Alma-Ata, 1971.

15. Judge, D.L. and R.W. Carlson, Science 183, 317 (1974).

16. Ridgway, S.T., Astrophys. J. 187, L41 (1974).

17. Treffers, R., H.P. Larson, U. Fink and T.N. Gautier, AAS Division for Planetary Sciences, 6 Ann. Meet: 17-21 Feb 1975, p. 17.

18. (Ridgway, S.T.), Sky and Tel. 50,215 (1975).

19. Owen, T., Science 167,1675 (1970).

20. Zharkov, V.N., V.P. Trubitsyn and L.V. Samsonenko, Fizika Zemli i planet [Physics of the Earth and Planets], Nauka Press, Moscow, 1971.

21. Hubbard, W.B., Astrophys. J. 162,687 (1970). /25

22. Allen, K.U., Astrofizicheskie velichiny [Astrophysical Quantities], Foreign Literature Publishing House, Moscow, 1960.

23. Zharkov, V.N., Vnutrenneye stroyeniye Zemli, Luny i planet [Internal Structure of the Earth, Moon and Planets], Znaniye Press, Moscow, 1973.

24. Lacy, J.H., A.T. Larrabee, E.R. Wollman et al., Astrophys. J. 198,L145 (1975).

25. Gillett, F.C., F.J. Low and W.A. Stein, Astrophys. J. 157, 925 (1969).

26. Hogan, J.S., S.I. Rasool and Th. Encrenaz, J.A.S. 26,898 (1969).

27. Wallace, L., M. Praether and M.S. Belton, Astrophys. J. 193,481 (1974).

28. Houck, J.R., J.B. Pollack, D. Schauk et al., Science 189, 720 (1975).

29. Westphal, J.A., Astrophys. J. 188,2, 112 (1974).

30. Gulkis, S., M.J. Klein and R.L. Poynter, IAU Symp. 65, 367 (1974).

31. Taranoga, O.G., Astron. zh. 52,380 (1975).

32. Sagan, C., J. Veverka et al., Science 185,901 (1974).

33. Rages, K., J. Veverka, L. Wasserman and K.C. Freeman, Icarus 23,59 (1974).

34. Vapillon, L., M. Combes and J.L. Lecacheux, Astron. and Astrophys. 29,135 (1973).

35. Hubbard, W.B., R.E. Nather, D.S. Evans et al., A.L. 77, 41 (1972).

36. Hubbard, W.B., D.M. Hunten and A. Kliore, Geophys. Res. L. 2,265 (1975).

37. Trafton, L.M. and P.H. Stone, Astrophys. J. 188,649 (1974).

38. Fjeldbo, G., COSPAR 18th plenary meeting, Varna, 1975.

39. Hubbard, W.B. and J.R. Jokipii, Sky and Tel. 50,212 (1975).

40. Shimizu, M., Icarus 14,273 (1971).

41. Capone, L.A. and S.S. Prasad, Icarus 20,200 (1973).

42. Vargaftik, N.B., Spravochnik po teplofizicheskim svoystvam gazov i zhidkostey [Handbook on Thermophysical Properties of Gases and Liquids], Nauka Press, Moscow, 1972.

43. Lewis, J.S., Icarus 10,365 (1969).

44. "Red coloring on Jupiter," Sky and Tel. 50,374 (1975).

45. Golitsyn, G.S., Vvedenie v dinamiky planetnykh atmosfer [Introduction to the Dynamics of Planetary Atmospheres] Gidrometeoizdat Press, Leningrad, 1973.

46. "Nasa Space Vehicle Design Criteria," SP 8069, 1972.

47. Bar-nun Akiva, Icarus 24,86 (1975).

48. Teŷfel', V.G., Atmosfera planety Yupiter,[Atmosphere of the Planet Jupiter], Nauka Press, Moscow, 1969.

49. Ingersoll, A.P., G. Münch, G. Neugebauer et al., Science 188,472 (1975).

50. Smith, E.J. et al., Science 188,451 (1975).

51. Frank, L.A., K.L. Ackerson, J.M. Wolfe and J.D. Mihalov, "Observations of plasmas in the Jovian magnetosphere," Preprint University of Iowa 75-5, Jan. 1975.

52. Trainer, J.H. et al., J. Geoph. Res. 79,3600 (1974).

53. Simpson, J.A. et al., J. Geoph. Res. 79,3522 (1974).

54. Van Allen, J.A. and D.N. Bauer, J. Geoph. Res. 79,3559 (1974).

55. Van Allen, J.A., B.A. Randoll et al., Science 188,459 (1975).

56. Fillius, R.W. and C.E. McIlwain, J. Geoph. Res. 79,3589 (1974).

57. Fillius, R.W. et al., Science 188,465 (1975).

58. Morrison, D. and D.P. Cruikshank, Space Sci. Rev. 15,641 (1974).

59. Soberman, R.K., S.L. Neste and K. Lichtenfeld, Science 183, 320 (1974).

60. Kinard, W.H., R.L. O'Neal, J.M. Alvarez and D.H. Humes, Science 183,321 (1974).

61. Humes, D.H., J.M. Alvarez, W.H. Kinard and R.L. O'Neal, Science 188,473 (1975).

62. di.Benedetto, F., Planet. Space Sci. 21,1605 (1973).

63. Lemekhova, E.N., Byull. ITA AN SSSR 14 3,(1975).

64. Morrison, D. and D.P. Cruikshank, Space Sci. Rev. 15,641 (1974).

TABLE 1. DIMENSIONS, MASS AND DENSITY OF JUPITER

Радиус экваториальный R_e, км[a]	71455 ± 30
Радиус полярный R_p, км[b]	66832 ± 30
Сжатие ε [c]	0.0647 ± 0.0001
Отношение массы Солнца к массе планеты [d]	1047.355 ± 0.025
Масса, кг [e]	$1.901 \cdot 10^{27}$
Средняя плотность, г.см$^{-3}$ [f]	1.33

Key: a. Equatorial radius Re, km
b. Polar radius Rp, km
c. Flattening ε
d. Ratio of solar mass to mass of planet
e. Mass, kg
f. Average density, g·cm^{-3}

TABLE 2. DISTANCE TO CENTER OF PLANET AND ACCELERATION OF GRAVITY AT P=1 ATM EQUIPOTENTIAL LEVEL VS. LATITUDE*

[a] Широта φ	[b] Расстояние до центра планеты R_φ, км	[c] Ускорение силы тяжести g м/сек^2
0	71455	22.60
10	71319	22.73
20	70912	23.13
30	70297	23.75
40	69547	24.55
50	68740	25.45
60	67989	26.36
70	67375	27.20
80	66975	27.90
90	66832	28.38

*Adopted nominal equatorial radius R_e=71455 km.
**With rotation taken into account

Key: a. Longitude
b. Distance to center of planet
c. Acceleration of gravity, m·sec^{-2} **

TABLE 3. PERIOD OF ROTATION

[a]Система отсчета долгот	[b]Область применения	[c]Период	[d]Линейная скорость вращения на экваторе, км/сек
I	[e]Оптический диапазон видимая поверхность облаков, $\varphi < 12^{\circ}$	$9^{h}50^{m}30^{s}.003$	12.38
II	[f]То же, $\varphi > 12^{\circ}$	$9^{h}55^{m}40^{s}.632$	12.27
III	[g]Радиодиапазон, магнитосфера	$9^{h}55^{m}29^{s}.37$	12.28

Key: a. Longitude system
b. Applicable region
c. Period
d. Linear velocity of rotation at equator, $km \cdot sec^{-1}$
e. Optical range, visible surface of clouds,
f. Same,
g. Radio range, magnetosphere

TABLE 4. MODEL OF CHEMICAL COMPOSITION OF ATMOSPHERE (GASES POSITIVELY DETECTED SPECTROSCOPICALLY)

[a]Газ	[b]Объемное содержание, %
[c]Водород H_2	86/*
[d]Гелий He	14/*
[e]Метан CH_4	0.04
[f]Ацетилен C_2H_2	$\sim 2 \cdot 10^{-6}$
[g]Этан C_2H_6	$\sim 10^{-4}$
[h]Аммиак NH_3	0.06
[i]Водяной пар H_2O	0.12
[j]Фосфин PH_3	/**

*In one model of atmosphere (II, see Tables 5 and 8), 50% H_2 and 50% He are assumed.

**There is qualitative identity [21] and no quantitative estimates to time of compilation of model.

Key: a. Gas
b. Volumetric content, %
c. Hydrogen
d. Helium
e. Methane
f. Acetylene
g. Ethane
h. Ammonia
i. Water vapor
j. Phosphine

TABLE 5. MODELS OF ATMOSPHERE OF JUPITER: BASIC PARAMETERS

[a] Модель	[b] Состав по объему	Средний молекулярный вес, μ c	[d] Температура, K				Средний градиент температуры в тропосфере K/км
			[e] на уровне P=1 атм	[f] минимум в стратопаузе (P≈0,1атм	мезосфера [g] (P=0,1мб)	термосфера [h] (P≈10^{-5}мб	
					g		i
1. Средняя	86% H_2, 14% He	2,28	180	120	160	600	2,2
11. Минимальная по T (максимальная по ρ в тропосфере)	50% H_2, 50% He	3,00	150	110	130	400	1.6
111. Максимальная по T (минимальная по ρ в тропосфере)	86% H_2, 14% He	2.28	220	125	260	800	2,2

Key: a. Model
b. Composition by volume
c. Average molecular weight, μ
d. Temperature, °K
e. At P=1 atm level
f. Minimum at stratopause
g. Mesosphere
h. Thermosphere
i. Average temperature gradient in troposphere, K/km
1. Average
11. Minimum T (maximum ρ in troposphere)
111. Maximum T (minimum ρ in troposphere)

TABLE 6. MODEL 1:

CHEMICAL COMPOSITION: 86% H_2, 14% He; $\mu = 2{,}28$; $R_e = 71455$ км

R_e, km	z, km	T, K	P, atm	ρ, kg/m^3
70755	-700	1672,4	1075	17,62
70805	-650	1569,0	869,4	15,18
70855	-600	1465,7	694,7	12,99
70905	-550	1362,4	545,0	10,96
70955	-500	1259,0	419,9	9,14
71005	-450	1155,6	316,6	7,51
71055	-400	1052,3	232,3	6,05
71105	-350	949,0	164,9	4,76
71155	-300	845,6	112,6	3,65
71205	-250	736,8	72,95	2,71
71255	-200	627,9	44,15	1,93
71275	-180	584,4	35,26	1,65
71295	-160	540,8	27,60	1,40
71315	-140	497,3	21,23	1,17
71335	-120	453,7	15,92	$9{,}62 \cdot 10^{-1}$
71355	-100	410,2	11,59	7,74
71365	-90	387,2	9,770	6,91
71375	-80	364,2	8,147	6,13
71385	-70	341,1	6,697	5,38
71395	-60	318,1	5,445	4,69
71405	-50	295,1	4,355	4,04
71415	-40	272,1	3,426	3,45
71425	-30	249	2,629	2,89
71435	-20	226	1,969	2,39
71445	-10	203	1,432	1,93

ORIGINAL PAGE IS
OF POOR QUALITY

TABLE 6 (continued)

R_e, km	z, km	T, K	P, atm	ρ, kg/m^3
71455	0	180	1,000	1,52
71465	10	163,9	$6,717 \cdot 10^{-1}$	1,12
71475	20	147,8	4,327	$8,02 \cdot 10^{-2}$
71485	30	131,7	2,651	5,52
71495	40	119,7	1,538	3,52
71505	50	128,3	$8,861 \cdot 10^{-2}$	1,89
71515	60	137,0	5,257	1,05
71525	70	145,6	3,241	$6,10 \cdot 10^{-3}$
71535	80	154,3	2,042	3,63
71545	90	160	1,348	2,31
71555	100	160	$5,723 \cdot 10^{-3}$	$9,80 \cdot 10^{-4}$
71575	120	160	2,430	4,16
71595	140	160	1,031	1,76
71615	160	160	$4,381 \cdot 10^{-4}$	$7,50 \cdot 10^{-5}$
71635	180	160	1,861	3,19
71655	200	160	$7,900 \cdot 10^{-5}$	1,35
71705	250	160	$9,281 \cdot 10^{-6}$	$1,59 \cdot 10^{-6}$
71755	300	160	1,090	$1,867 \cdot 10^{-7}$

[Translator's note : commas in tabulated figures are equivalent to decimal points.]

TABLE 6 (continued)

R_e, км	z, км	T, K	$P(H_2)$, атм	$\rho(H_2)$, $\frac{кг}{м^3}$	P(He), атм	ρ(He), $\frac{кг}{м^3}$	$P(H_2+He)$, атм	$\rho(H_2+He)$ $\frac{кг}{м^3}$
71755	300	160	$9,374\cdot10^{-7}$	$1,408\cdot10^{-7}$	$1,526\cdot10^{-7}$	$4,585\cdot10^{-8}$	$1,090\cdot10^{-6}$	$1,87\cdot10^{-7}$
71774	319	160	$4,592$	$6,90\cdot10^{-8}$	$3,661\cdot10^{-8}$	$1,10$	$4,958\cdot10^{-7}$	$8,00\cdot10^{-8}$
71800	345	180,1	1,824	2,43	$5,772\cdot10^{-9}$	$1,54\cdot10^{-9}$	1,882	2,58
71855	400	261,6	$4,089\cdot10^{-8}$	$3,76\cdot10^{-9}$	$2,796\cdot10^{-10}$	$5,14\cdot10^{-11}$	$4,117\cdot10^{-8}$	$3,81\cdot10^{-9}$
71905	450	335,6	1,488	1,06	$3,701\cdot10^{-11}$	$5,30\cdot10^{-12}$	1,492	1,06
71955	500	409,7	$6,618\cdot10^{-9}$	$3,88\cdot10^{-10}$	$7,324\cdot10^{-12}$	$8,59\cdot10^{-13}$	$6,625\cdot10^{-9}$	$3,89\cdot10^{-10}$
72005	550	483,8	3,367	1,67	1,897	1,88	3,369	1,67
72055	600	557,7	1,890	$8,14\cdot10^{-11}$	$5,975\cdot10^{-13}$	$5,15\cdot10^{-14}$	1,891	$8,14\cdot10^{-11}$
72057	602	560,7	1,852	7,93	5,736	4,92	1,853	7,93
72123	668	600	$9,348\cdot10^{-10}$	3,74	1,461	1,17	$9,349\cdot10^{-10}$	3,74
72155	700	600	6,784	2,72				
72255	800	600	2,492	$9,98\cdot10^{-12}$				
72355	900	600	$9,152\cdot10^{-11}$	3,67				
72455	1000	600	3,361	1,35				
72555	1100	600	1,234	$4,94\cdot10^{-13}$				
72655	1200	600	$4,534\cdot10^{-12}$	1,82				

ORIGINAL PAGE IS
OF POOR QUALITY

TABLE 7. MODEL 111:

CHEMICAL COMPOSITION: 86% H_2, 14% He; $\mu = 2,28$, $g = 25$м/сек^2

R_e, км	z, km	T, K	P, atm	ρ, kg/м^3
70655	-800	1919,1	913,5	13.04
70705	-750	1815,8	764,7	11,54
70755	-700	1712,4	630,5	10,09
70805	-650	1609,0	513,6	8.75
70855	-600	1505,7	411,6	7,49
70905	-550	1402,4	324,9	6,35
70955	-500	1299,0	251,9	5,31
71005	-450	1195,6	191,6	4,39
71055	-400	1092,3	142,3	3,57
71105	-350	989,0	102,5	2,84
71155	-300	885,6	71,08	2,20
71205	-250	776,8	47,06	1,66
71255	-200	667,9	29,25	1,20
71275	-180	624,4	23,64	1,04
71295	-160	580,8	18,83	$8.88 \cdot 10^{-1}$
71315	-140	537,3	14,74	7,52
71335	-120	493,7	11,31	6,28
71355	-100	450,2	8,448	5,14
71365	-90	427,2	7,228	4,64
71375	-80	404,1	6,128	4,15
71385	-70	381,1	5,139	3,70
71395	-60	358,1	4,274	3,27
71405	-50	335,1	3.503	2,86
71415	-40	312,1	2,833	2,49
71425	-30	289,1	2,254	2,14

TABLE 7. (continued)

$R_\odot$, км	z, км	T, K	P, атм	ρ, кг/м^3
71435	−20	266,0	1,759	1,81
71445	−10	243,0	1,343	1,51
71455	0	220	1,000	1,24
71465	10	200,2	$7{,}213\cdot10^{-1}$	$9{,}87\cdot10^{-2}$
71475	20	180,4	5,028	7,64
71485	30	160,6	3,365	5,74
71495	40	140,8	2,132	4,15
71505	50	125	1,274	2,79
71515	60	130	$7{,}450\cdot10^{-2}$	1,57
71525	70	145,2	4,528	$8{,}55\cdot10^{-3}$
71535	80	156,1	2,878	5,05
71545	90	167,1	1,883	3,09
71555	100	178,0	1,268	1,95
71575	120	196,0	$6{,}094\cdot10^{-3}$	$8{,}52\cdot10^{-4}$
71595	140	210	3,114	4,06
71615	160	224	1,649	2,02
71635	180	235	$9{,}082\cdot10^{-4}$	1,06
71655	200	246	5,118	$5{,}70\cdot10^{-5}$
71705	250	260	1,316	1,39
71755	300	260	$3{,}526\cdot10^{-5}$	$3{,}72\cdot10^{-6}$
71805	350	240	$9{,}007\cdot10^{-6}$	1,03
71855	400	220	2,029	$2{,}527\cdot10^{-7}$

TABLE 7. (continued).

R_e, km	z, km	T, K	$P(H_2)$, atm	$\rho(H_2)$, $\frac{kg}{m^3}$	P(He), atm	ρ(He), $\frac{kg}{m^3}$	$P(H_2+He)$, atm	$\rho(H_2+He)$, $\frac{kg}{m^3}$
71855	400	220,0	$1,745 \cdot 10^{-6}$	$1,907 \cdot 10^{-7}$	$2,841 \cdot 10^{-7}$	$6,208 \cdot 10^{-8}$	$2,029 \cdot 10^{-6}$	$2,53 \cdot 10^{-7}$
71902	447	220	$4,833 \cdot 10^{-7}$	$5,28 \cdot 10^{-8}$	$2,179 \cdot 10^{-8}$	$4,76 \cdot 10^{-9}$	$5.051 \cdot 10^{-7}$	$5,75 \cdot 10^{-8}$
71938	483	254,8	1,945	1,83	$3,527 \cdot 10^{-9}$	$6,65 \cdot 10^{-10}$	1,980	1,90
71955	500	278,4	1,324	1.14	1.619	2,80	1,340	1,42
72005	550	347,9	$5,047 \cdot 10^{-8}$	$3,49 \cdot 10^{-9}$	$2,353 \cdot 10^{-10}$	$3,25 \cdot 10^{-11}$	$5,070 \cdot 10^{-8}$	$3,52 \cdot 10^{-9}$
72055	600	417,4	2,294	1,32	$4,861 \cdot 10^{-11}$	$5,60 \cdot 10^{-12}$	2,299	1,32
72155	700	556,4	$6,618 \cdot 10^{-9}$	$2,86 \cdot 10^{-10}$	$4,042 \cdot 10^{-12}$	$3,49 \cdot 10^{-13}$	$6,622 \cdot 10^{-9}$	$2,86 \cdot 10^{-10}$
72255	800	695,4	2,523	$8.72 \cdot 10^{-11}$	$5,872 \cdot 10^{-13}$	$4.06 \cdot 10^{-14}$	2,524	$8,72 \cdot 10^{-11}$
72287	832	739,9	1,930	6,26	3,438	2,23	1,930	6,26
72355	900	785,8	1,130	3,45				
72376	921	800,0	$9,632 \cdot 10^{-10}$	2,89				
72455	1000	800	5,321	1,60				
72555	1100	800	2,511	$7,54 \cdot 10^{-12}$				
72655	1200	800	1,185	3,56				
72755	1300	800	$5,590 \cdot 10^{-11}$	1,68				
72855	1400	800	2,637	$7,92 \cdot 10^{-13}$				
72955	1500	800	1,245	3,74				
73055	1600	800	$5,872 \cdot 10^{-12}$	1,76				
73155	1700	800	2,771	$8,32 \cdot 10^{-14}$				

ORIGINAL PAGE IS
OF POOR QUALITY

TABLE 8. MODEL 11;

CHEMICAL COMPOSITION: 50% H_2, 50% He, $\mu = 3{,}00$, $g = 25$м/сек^2

r_e, км	z, км	T, K	P, атм	ρ, kg/м^3
71215	-240	529,7	1310	89.18
71235	-220	498,0	923,0	66,84
71255	-200	466,4	634,2	40,04
71275	-180	434,8	424,4	35,20
71295	-160	403,1	275,2	24,62
71315	-140	371,5	173,0	16,79
71335	-120	339,8	104,2	11,06
71355	-100	308,2	59,91	7,01
71365	-90	292,4	44,41	5,48
71375	-80	276,6	32,38	4,22
71385	-70	260,7	23,11	3,20
71395	-60	244,9	16,24	2,39
71405	-50	229,1	11,09	1,75
71415	-40	213,3	7,386	1,25
71425	-30	197,5	4,765	$8.70 \cdot 10^{-1}$
71435	-20	181,6	2,963	5,88
71445	-10	165,8	1,767	3,84
71455	0	150,0	1,000	2,40
71465	10	138,8	$5{,}332 \cdot 10^{-1}$	1,38
71475	20	127,7	2,719	$7{,}68 \cdot 10^{-2}$
71485	30	116,5	1,297	4,01
71495	40	110,0	$5{,}856 \cdot 10^{-2}$	1.92
71505	50	118,9	2,665	$8{,}88 \cdot 10^{-3}$
71515	60	127,8	1,282	3,62
71525	70	130,0	$6{,}437 \cdot 10^{-3}$	1,78

TABLE 8 (continued)

$R_\oplus$, km	z, km	T, K	P, атм	ρ, kg/m^3
71535	80	130	3,218	$8,93 \cdot 10^{-4}$
71545	90	130	1,608	4,46
71555	100	130	$8,037 \cdot 10^{-4}$	2,23
71575	120	130	2,007	$5,57 \cdot 10^{-5}$
71595	140	130	$5,016 \cdot 10^{-5}$	1,39
71615	160	130	1,253	$3,48 \cdot 10^{-6}$
71635	180	130	$3,130 \cdot 10^{-6}$	$8,68 \cdot 10^{-7}$
71655	200	130	$7,818 \cdot 10^{-7}$	2,168

ORIGINAL PAGE IS
OF POOR QUALITY

TABLE 8 (continued)

R_e, km	z, km	T, K	$P(H_2)$, atm	$\rho(H_2)$, $\frac{kg}{m^3}$	P(He), atm	ρ(He), $\frac{kg}{m^3}$	$P(H_2+He)$, atm	$\rho(H_2+He)$, $\frac{kg}{m^3}$
71655	200	130,0	$3,909 \cdot 10^{-7}$	$7,23 \cdot 10^{-8}$	$3,909 \cdot 10^{-7}$	$1,44 \cdot 10^{-7}$	$7,818 \cdot 10^{-7}$	$2,16 \cdot 10^{-7}$
71661	206	130	2,895	5,35	2,143	$7,92 \cdot 10^{-8}$	5,038	1,33
71676	221	140,2	1,144	1,91	$3,349 \cdot 10^{-8}$	1.15	1,479	$3,06 \cdot 10^{-8}$
71705	250	177,0	$3,796 \cdot 10^{-8}$	$5,16 \cdot 10^{-9}$	$3,686 \cdot 10^{-9}$	$1,00 \cdot 10^{-9}$	$4,165 \cdot 10^{-8}$	$6,16 \cdot 10^{-9}$
71755	300	240,4	$8,904 \cdot 10^{-9}$	$8,90 \cdot 10^{-10}$	$2,027 \cdot 10^{-10}$	$4,05 \cdot 10^{-11}$	$9.107 \cdot 10^{-9}$	$9,31 \cdot 10^{-10}$
71805	350	303,8	2,932	2,32	$2,198 \cdot 10^{-11}$	$3,48 \cdot 10^{-12}$	2,954	2,36
71855	400	367,2	1,193	$7,80 \cdot 10^{-11}$	$3,638 \cdot 10^{-12}$	$4,76 \cdot 10^{-13}$	1,197	$7,85 \cdot 10^{-11}$
71857	402	369,7	1,154	7,50	3,407	4,43	1,157	7,54
71902	447	400,0	$5,728 \cdot 10^{-10}$	3,44	$8,383 \cdot 10^{-13}$	1,08	$5,736 \cdot 10^{-10}$	3,45
71955	500	400	2,583	1,55				
72055	600	400	$5,750 \cdot 10^{-11}$	$3,46 \cdot 10^{-12}$				
72155	700	400	1,280	$7,69 \cdot 10^{-13}$				
72255	800	400	$2,849 \cdot 10^{-12}$	1,71				
72355	900	400	$6,342 \cdot 10^{-13}$	$3,81 \cdot 10^{-14}$				
72455	1000	400	1,411	$8,47 \cdot 10^{-15}$				

ORIGINAL PAGE IS
OF POOR QUALITY

TABLE 9. INTENSITY OF ILLUMINATION, ALBEDO, BRIGHTNESS

a Длина волны, мкм	b Освещенность на верхней границе облачного слоя/* 10^{-3} Вт.см$^{-2}$мкм$^{-1}$	c Геометрическое альбедо	d Средняя яркость/** облачного слоя 10^{-4} Вт.см$^{-2}$стер$^{-1}$ мкм$^{-1}$
0,3	1,60	0,25	1,28
0,4	4,03	0,37	4,74
0,5	5,19	0,48	7,93
0,6	4,76	0,54	8,17
0,7	3,78	0,44	5,30
0,8	2,95	0,37	3,47
1,0	1,90	0,3	2,22
1,25	1,32	~0,4	1,68
1,5	0,70	0,15	0,34
1,6	0,58	0,4	0,74
1,8	0,40	~0,03	~0,04
2,0	0,27	~0,1	~0,09
2,3	0,20	~0,03	~0,02
2,4	0,16	0,05	~0,03
2,7	0,10	0,3	~0,10
3,0	0,05	~0,03	~0.005.

*Sun height above horizon 45°.
**Sun height above horizon 45°, phase angle 0°.

Key: a. Wavelength, μm
b. Intensity of illumination at upper boundary of cloud layer,* 10^{-3} W·cm^{-2}·μm^{-1}
c. Geometric albedo
d. Average brightness of cloud layer,** 10^{-4} W·cm^{-2}·ster^{-1}·μm^{-1}

TABLE 10. TYPICAL DARK AND BRIGHT FIELD CONTRAST

[a] Длина волны, Å	[illegible]	[illegible]	5940	6480
[b] Отношение яркостей темных полос и наиболее яркой светлой зоны	0,80-0,88	0,82-0,88	0,88-0,97	0,92-0,98

Key: a. Wavelength, A

b. Ratio of dark band brightness and brightest light zone

TABLE 11

[a] Область	[b] Локализация в магнитосфере R_e	[c] [illegible] $см^{-3}$	[d] кТ, эВ	[e] Интенсивность
Плазмосфера [f]	2,8-6	50-100	100	[g] $10^8 см^{-2} сек^{-1} ст^{-1}$ или $10^9 см^{-2} сек^{-1}$
Спорадическая область [h]	6 - 8	1 - 10	400	[i] $3 \cdot 10^7 см^{-2} сек^{-1}$
[j] Кольцевой ток	8 - 15	10 - 15	400	и падает до $6 \cdot 10^6 см^{-2} сек^{-1}$
Плазменный [k] слой	15 - 25	1	400	на 11 R_e

Key: a. Region
b. Location in magnetosphere, c.
d. kT, eV
e. Intensity
f. Plasmasphere
g. 10^8 $cm^{-2} \cdot sec^{-1} \cdot ster^{-1}$ or 10^9 $cm^{-2} \cdot sec^{-1}$
h. Sporadic region
i. $3 \cdot 10^7$ $cm^{-2} \cdot sec^{-1}$ and falls to $6 \cdot 10^6$ $cm^{-2} \cdot sec^{-1}$ at 11 R_e
j. Ring current
k. Plasma layer

ORIGINAL PAGE IS
OF POOR QUALITY

TABLE 12

a E, МэВ	Область наблюдения интенсивных потоков, R_e b	Спад интенсивности на два-три порядка, R_e c	Положение максимума, R_e d	Интенсивность $см^{-2} \cdot сек^{-1}$ e	Примечание f
		g электроны			
>0.015	<15	>15	1.6	$3 \cdot 10^9$	
>0.04	3-15	15-20	1.6	$5 \cdot 10^6 \div 3 \cdot 10^7$	
>0.16	2.8-13	>13	3.7	$3 \cdot 10^7 - 10^8$	h
>0.55	2.8-8	10-13	3.7	10^8	Уменьшение интенсивности на порядок вблизи орбиты спутников Юпитера
>3			1.8	$1,6 \cdot 10^8$	
>5	2.8-8	10-13	3.4	$5 \cdot 10^6 - 5 \cdot 10^8$	
>8	1,6-15	>15	1.6	$10^5 - 2 \cdot 10^7$	
>21	3,4-5	5-10	3.7	$(3 \div 5) \cdot 10^7$	
>35	1.6-10	>11	1.6	$4 \cdot 10^3 \div 5 \cdot 10^6$	
		i протоны			
0.5-2.1	1.6-25	>25	1.6	$(1 \div 6) \cdot 10^6$	j Быстрый спад интенсивности до 10^3
>5	3,4	3,4-10	3,4	$6 \cdot 10^6$	
>20	1.6	3-9	1,6	10^5	

Key: a. E, MeV
b. Intense current observation region, Re
c. 2-3 order of magnitude intensity drop, Re
d. Location of maximum, Re
e. Intensity, $cm^{-2} \cdot sec^{-1}$
f. Note
g. Electrons
h. Order of magnitude decrease of intensity near Jovian satellite orbits
i. Protons
j. Rapid intensity drop to 10^3

TABLE 13. METEORITE FLUXES

Zone A. Interplanetary Space Between Earth and Jupiter (Including Asteroid Belt) Outside Region of Increased Concentration Near Jupiter

a Радиус, см	b Масса, г	c Поток, $м^{-2}$, $сут^{-1}$		
		d средняя модель	e минимальная модель	f максимальная модель
$4 \cdot 10^{-4}$	$8 \cdot 10^{-10}$	$1{,}0 \cdot 10^{-1}$	$2{,}5 \cdot 10^{-2}$	$4{,}0 \cdot 10^{-1}$
$1 \cdot 10^{-3}$	$1{,}2 \cdot 10^{-8}$	$5{,}0 \cdot 10^{-2}$	$1{,}2 \cdot 10^{-2}$	$2{,}0 \cdot 10^{-1}$
$1 \cdot 10^{-2}$	$1{,}2 \cdot 10^{-5}$	$1{,}5 \cdot 10^{-3}$	$3{,}9 \cdot 10^{-4}$	$6{,}0 \cdot 10^{-3}$
$1 \cdot 10^{-1}$	$1{,}2 \cdot 10^{-2}$	$2{,}5 \cdot 10^{-5}$	$6{,}0 \cdot 10^{-6}$	$1{,}0 \cdot 10^{-4}$
1	12	$2{,}0 \cdot 10^{-7}$	$5{,}0 \cdot 10^{-8}$	$8{,}0 \cdot 10^{-7}$
10	12000	$1{,}0 \cdot 10^{-9}$	$2{,}5 \cdot 10^{-10}$	$4{,}0 \cdot 10^{-9}$

Zone B. Region of Increased Meteorite Concentration Near Jupiter (Radius About 10^7 km)

a Радиус, см	b Масса, г	c Поток, $м^{-2}$ $сут^{-1}$		
		d средняя модель	e минимальная модель	f максимальная модель/*
$4 \cdot 10^{-4}$	$8 \cdot 10^{-10}$	$1{,}0$	$1{,}0 \cdot 10^{-1}$	10
$1 \cdot 10^{-3}$	$1{,}2 \cdot 10^{-8}$	$5{,}0 \cdot 10^{-1}$	$5{,}0 \cdot 10^{-2}$	$5{,}0$
$1 \cdot 10^{-2}$	$1{,}2 \cdot 10^{-5}$	$1{,}5 \cdot 10^{-2}$	$1{,}5 \cdot 10^{-3}$	$1{,}5 \cdot 10^{-1}$
$1 \cdot 10^{-1}$	$1{,}2 \cdot 10^{-2}$	$2{,}5 \cdot 10^{-4}$	$2{,}5 \cdot 10^{-5}$	$2{,}5 \cdot 10^{-3}$
1	12	$2{,}0 \cdot 10^{-6}$	$2{,}0 \cdot 10^{-7}$	$2{,}0 \cdot 10^{-5}$
10	12000	$1{,}0 \cdot 10^{-8}$	$1{,}0 \cdot 10^{-9}$	$1{,}0 \cdot 10^{-7}$

*Probability for inner part of zone (distance from Jupiter less than 10^6 km).

Key: a. Radius, cm
b. Mass, g
c. Flux, $m^{-2} \cdot day^{-1}$
d. Average model
e. Minimum model
f. Maximum model

TABLE 14. SATELLITES OF JUPITER

[a] Спутник	[b] Расстояние от планеты, тыс. км	Сидерический период, сутки [c]	Синодический период обращения [d]	[e] Наклонение орбиты */**	Эксцентриситет орбиты [f]	Радиус, км [g]	Звездная величина $V(1,0)$ */** [h]
1. Ио	421,8	1,769	$1^d\,18^h\,28^m\,36^s$	0P	Малый [i]	1820±10	-1,68
2. Европа	671,4	3,551	$3^d\,13^h\,17^m\,54^s$	0P	и пе-	1550±150	-1,48
3. Ганимед	1071	7,154	$7^d\,03^h\,59^m\,36^s$	0P	ремен-	2635±25	-2,09
4. Каллисто	1884	16,689	$16^d\,18^h\,05^m\,07^s$	0P	ный	2500±150	-1,05
5. Амальтея	181	0,498	$11^h\,57^m\,28^s$	0P	0,003	≈100	+6,3
6. Гестия	11500	250,62	260,0 [d]	28,5B	0,155	≈80	+8,0
7. Гера	11750	259,8	276,1	28,0B	0,207	≈30	+9,3
8. Посейдон	23500	733,9	631,0	R33B	0,38	≈ 8	+12,1
9. Гадес	23700	755	626	R24B	0,25	≈10	+11,1
10. Деметра	11750	260	276	28,3B	0,140	≈ 9	+11,9
11. Пан	22500	696	599	R16,6B	0,207	≈11	+11,14
12. Андратея	21000	625	546	R	0,13	≈ 8	+12,1
13. № I3	-	-	-	-	-	≈ 5	+13

*P. inclination to equatorial plane of planet; B. inclination of orbital plane; R. retrograde rotation
**V(1.0) visual star magnitude in phase zero, reduced to sun-planet and planet-observer distances 1 AU.

Key: a. Satellite
b. Distance from planet, km
c. Sidereal period, days
d. Synodic period of rotation
e. Inclination of orbit
f. Eccentricity of orbit
g. Radius, km
h. Star magnitude, V (1.0)
i. Small and variable
1. Io
2. Europa
3. Ganymede
4. Callisto
5. Almathea
6. Hestia
7. Hera
8. Poseidon
9. Hades
10. Demeter
11. Pan
12. Andrathea

ORIGINAL PAGE IS OF POOR QUALITY

TABLE 15. ASTRO DYNAMIC CONSTANTS CONNECTED WITH GALILEAN SATELLITE SYSTEM OF JUPITER

[a] Параметр	[b] Ио	[c] Европа	[d] Ганимед	[e] Каллисто
a, km	421758,59	671049,78	1070416,65	1882714,11
e	0,00001	0,00013	0,00139	0,00736
i, град [f]	0,032	0,467	0,179	0,245
ω, град [f]	266,5000 + 0,14875406·T	161,8000 + 0,03980417·T	114,2000 + 0,00707249·T	317,2000 + 0,00186251·T
Ω, град [f]	171,6000 − 0,13111940·T	57,5000 − 0,03228959·T	190,5000 − 0,00680967·T	340,8000 − 0,00156486·T
λ, град [f]	338,7734 + 203,488954597T	285,5142 + 101,374723597T	348,8846 + 50,317608097T	325,9951 + 21,571071977T
μ	5950±75	3250±75	9940±100	7100±215

Key: a. Parameter
b. Io
c. Europa
d. Ganymede
e. Callisto
f. degrees

TABLE 16. GALILEAN SATELLITE OF JUPITER, BASIC PHYSICAL CHARACTERISTICS

[a] Характеристики	[b] Ио	[c] Европа	[d] Ганимед	[e] Каллисто
[f] Радиус, км	I820±I0	I550±I50	2635±25	2500±I50
Масса [6]: [g] спутник/Юпитер, $I0^{-5}$ [h]	(4,469±0,06)	(2,565±0,06)	(7,845±0,08)	(5,603±0,I7)
кг [i]	8,496·$I0^{22}$	4,876·$I0^{22}$	I,49I·$I0^{23}$	I,065·$I0^{23}$
Средняя плотность, г/см^3 [j]	3,36	3,I2	I,95	I,63
Геометрическое альбедо [64] [k]				
3I90 Å	0,I3	0,53	0,28	0,II
4330 Å	0,4C	0,56	0,38	0,I5
5640 Å	0,62	0,68	0,43	0,I9
7300 Å	0,7I	0,68	0,44	0,2I
IIIOI Å	0,75	0,62	0,42	0,2I
Атмосферное давление у поверхности, атм [l]	$I0^{-8}$ /* $-I0^{-7}$	/**	$I0^{-6}$ Р $I0^{-3}$	/**
Вероятный состав атмосферы [m]	NH_3, N_2, H_2	/**	NH_3, N_2, H_2	/**
Яркостная температура поверхности, [64] [n]: 8-I4мкм [o]	I38±4 К	I30±4 К	I42±4 К	I52±4 К
I7-28мкм [o]	I27±4 К	I20±4 К	I37±5 К	I50±6 К
Вероятный состав грунта [p]	[q] снег H_2O	[q] снег H_2O	[r] снег H_2O+ силикатные частицы	[r] снег H_2O+ силикатные частицы
Вероятный состав недр [s]	[t] силикаты	[t] силикаты	[u] льды H_2O, NH_3 и др. ~I0% силикатов	[u] льды H_2O, NH_3 и др. ~I0% силикатов

*Ionosphere detected ($n_e=10^5$ at altitude of about 100 km)
**No data

Key: TABLE 16 (continued)

Key:
a. Characteristics
b. Io
c. Europa
d. Ganymede
e. Callisto
f. Radius, km
g. Mass
h. Satellite/Jupiter, 10^{-5}
i. kg
j. Average density, $g \cdot cm^{-3}$
k. Geometric albedo
l. Atmospheric pressure at surface, atm
m. Probable composition of atmosphere
n. Brightness temperature of surface
o. μm
p. Probable composition of soil
q. H_2O snow
r. H_2O snow plus silicate particles
s. Probable interior composition
t. Silicates
u. H_2 ice, NH_3, etc. ~10% silicates

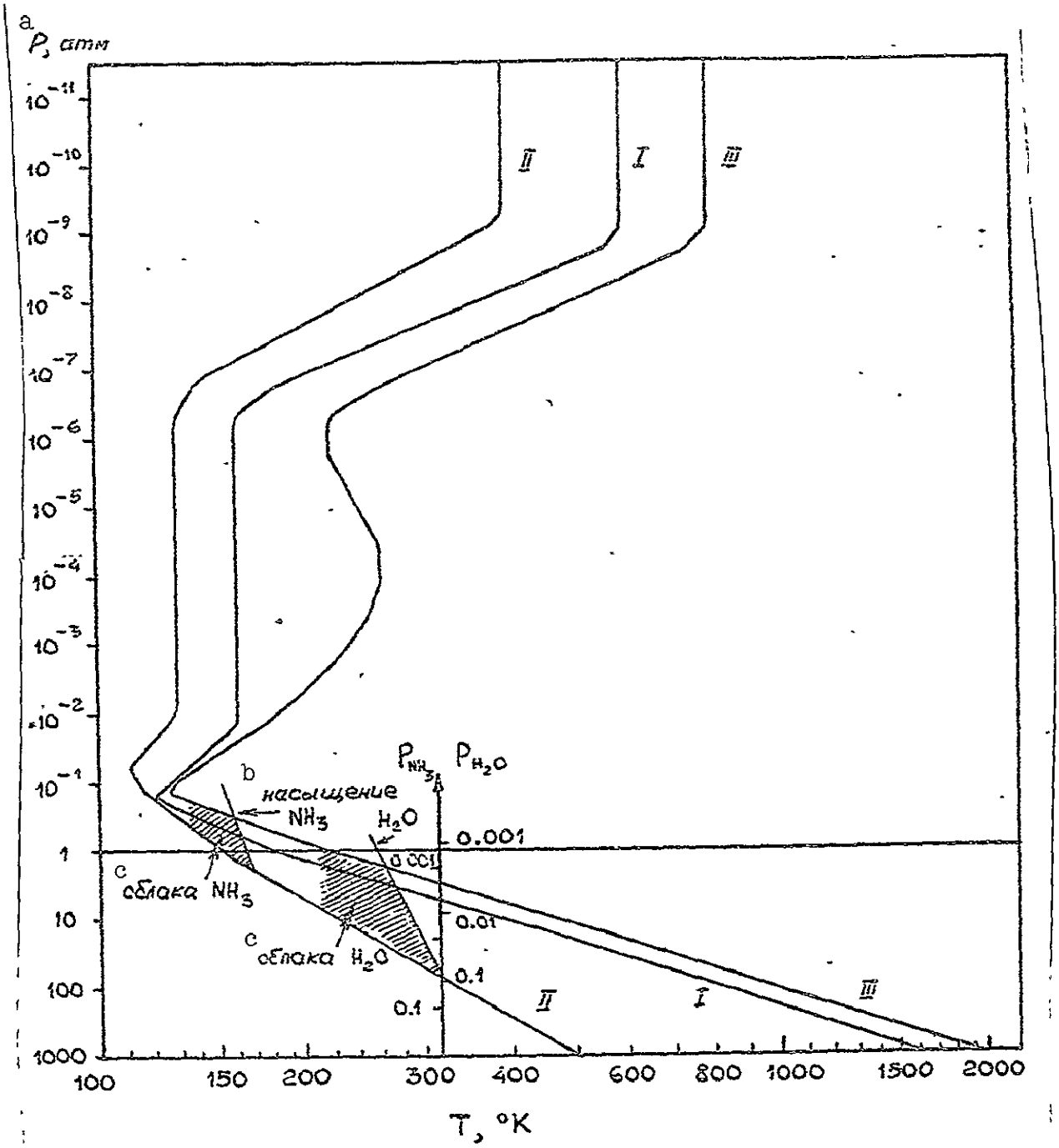

Fig. 1. Function P(T) in three models of atmosphere: NH_3 and H_2O saturation levels corresponding to lower boundaries of ammonia and water clouds are shown.

Key: a. P, atm
b. Saturation
c. Clouds

ORIGINAL PAGE IS
OF POOR QUALITY

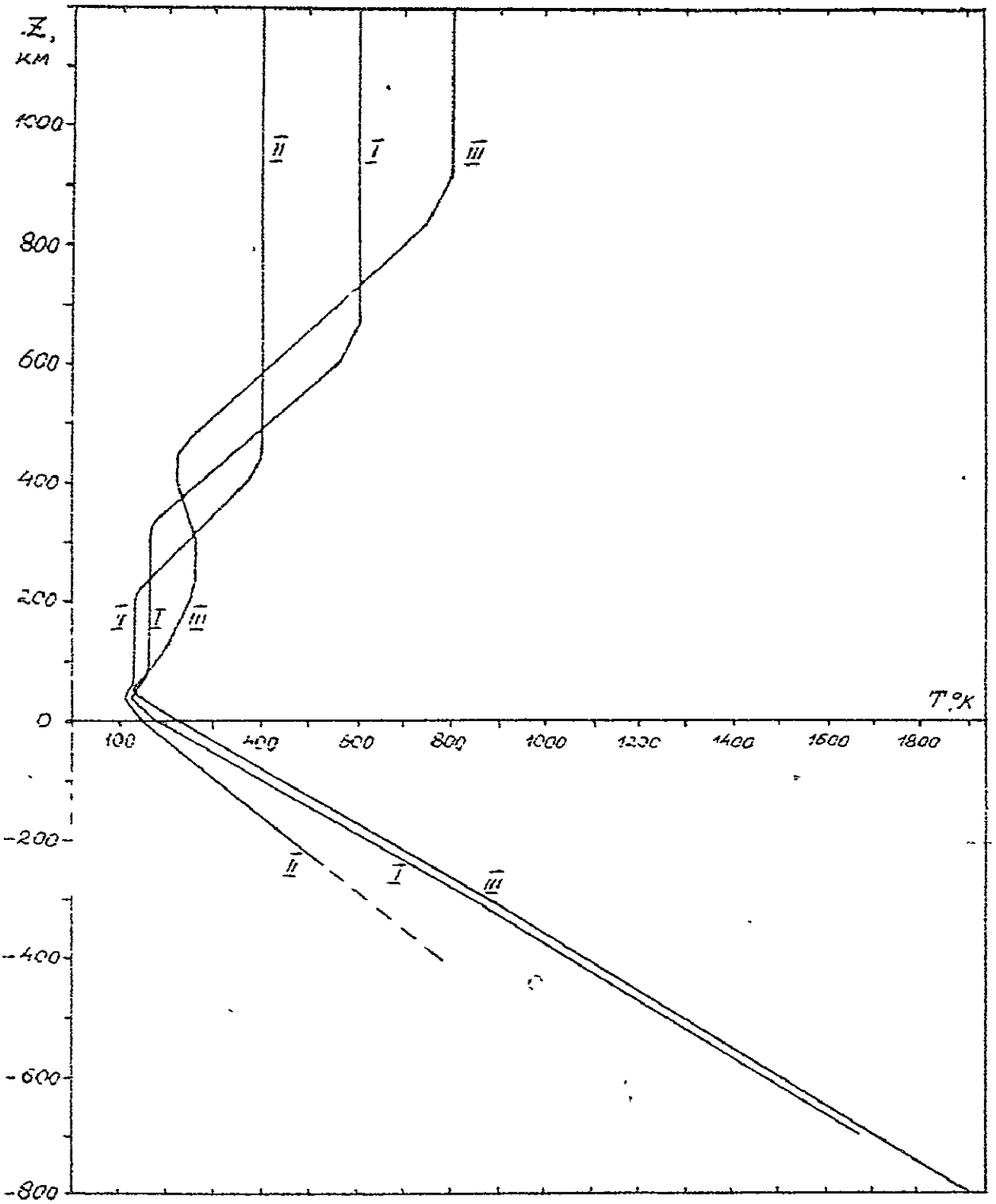

Fig. 2. Temperature T vs. altitude in models I-III.

ORIGINAL PAGE IS
OF POOR QUALITY

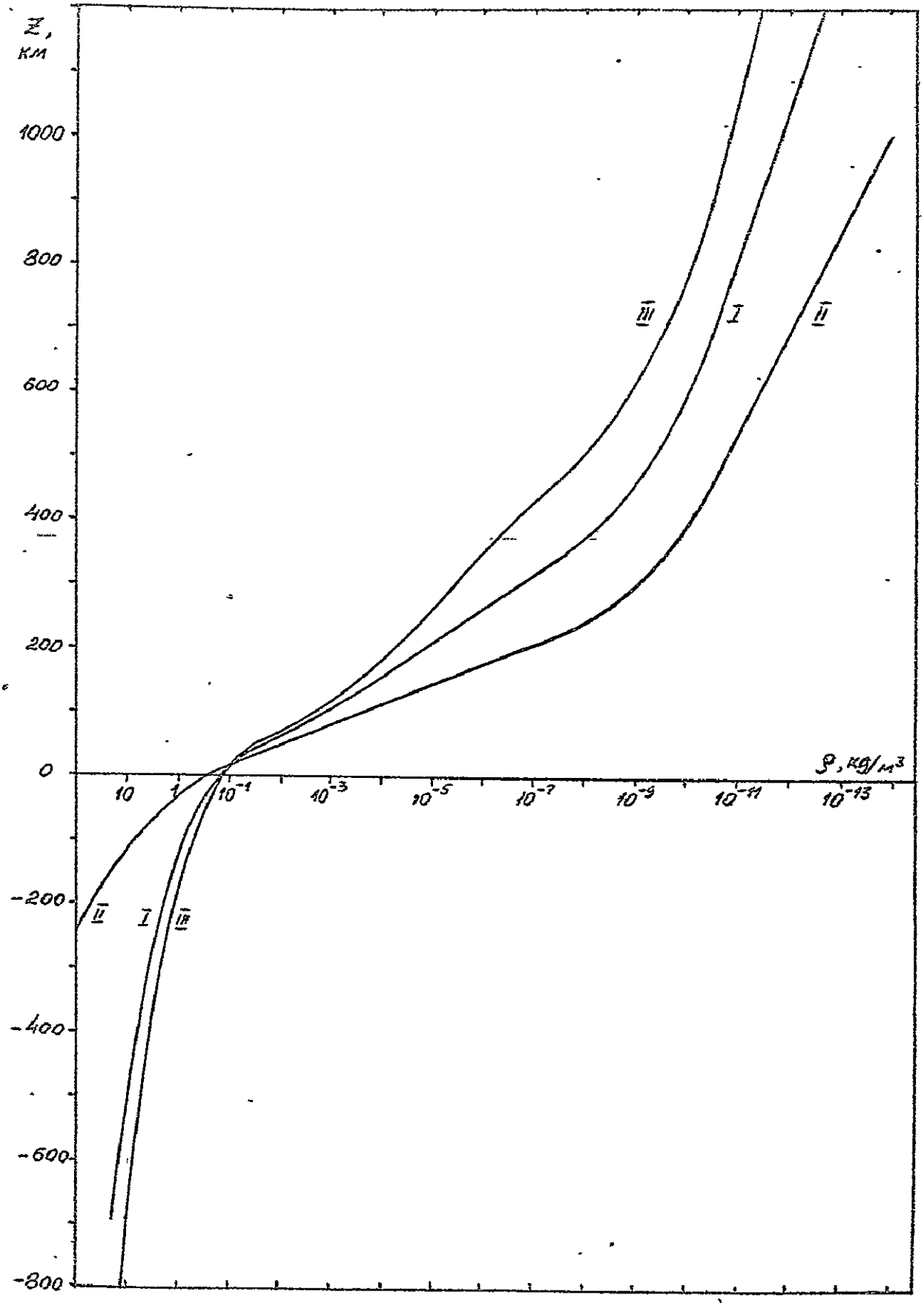

Fig. 3. Density ρ vs. altitude in models I-III.

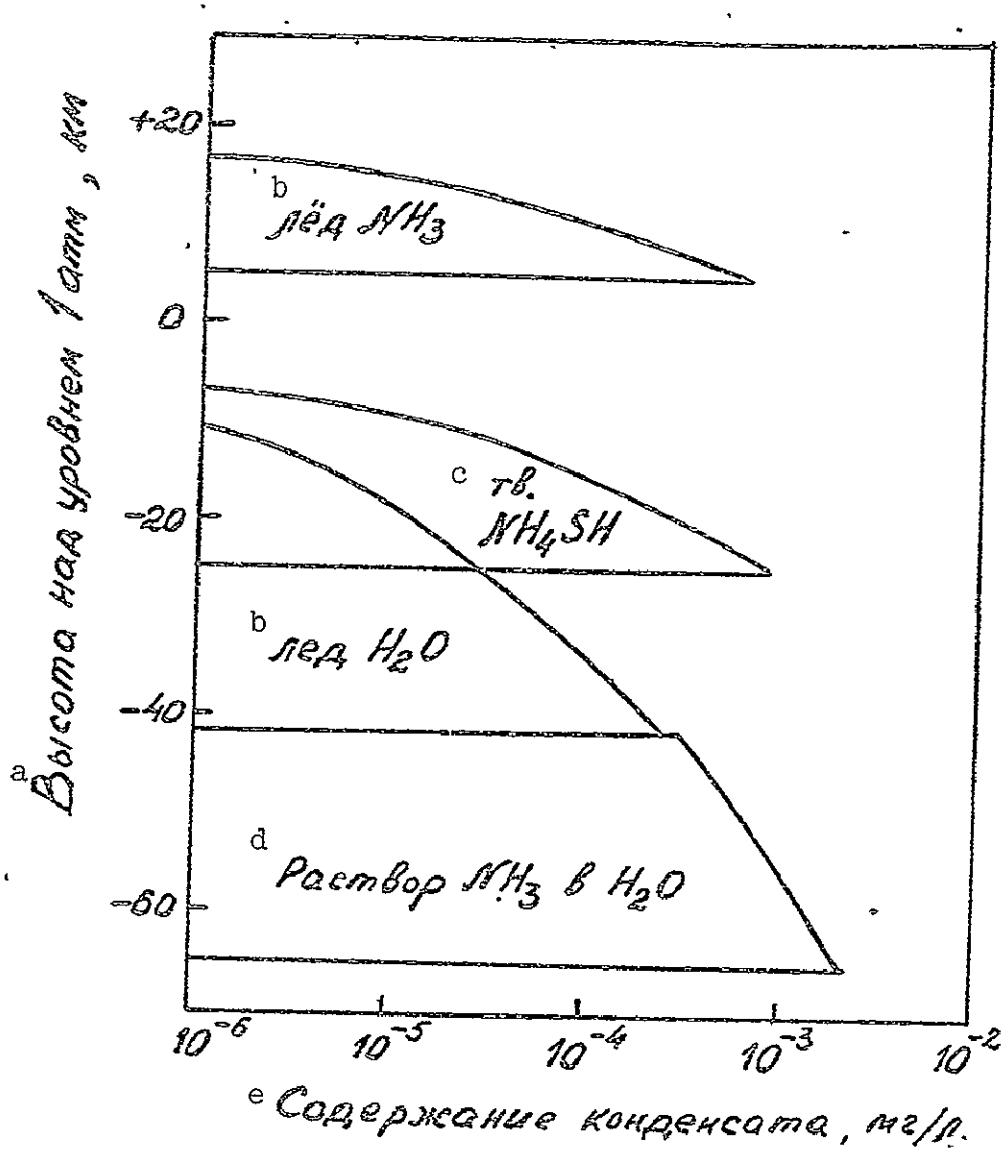

Fig. 4. Diagram of possible cloud structure on Jupiter.

Key: a. Altitude above 1 atm level, km
b. Ice
c. Solid
d. NH_3 solution in H_2O
e. Condensate content, mg/ℓ

ORIGINAL PAGE IS
OF POOR QUALITY.

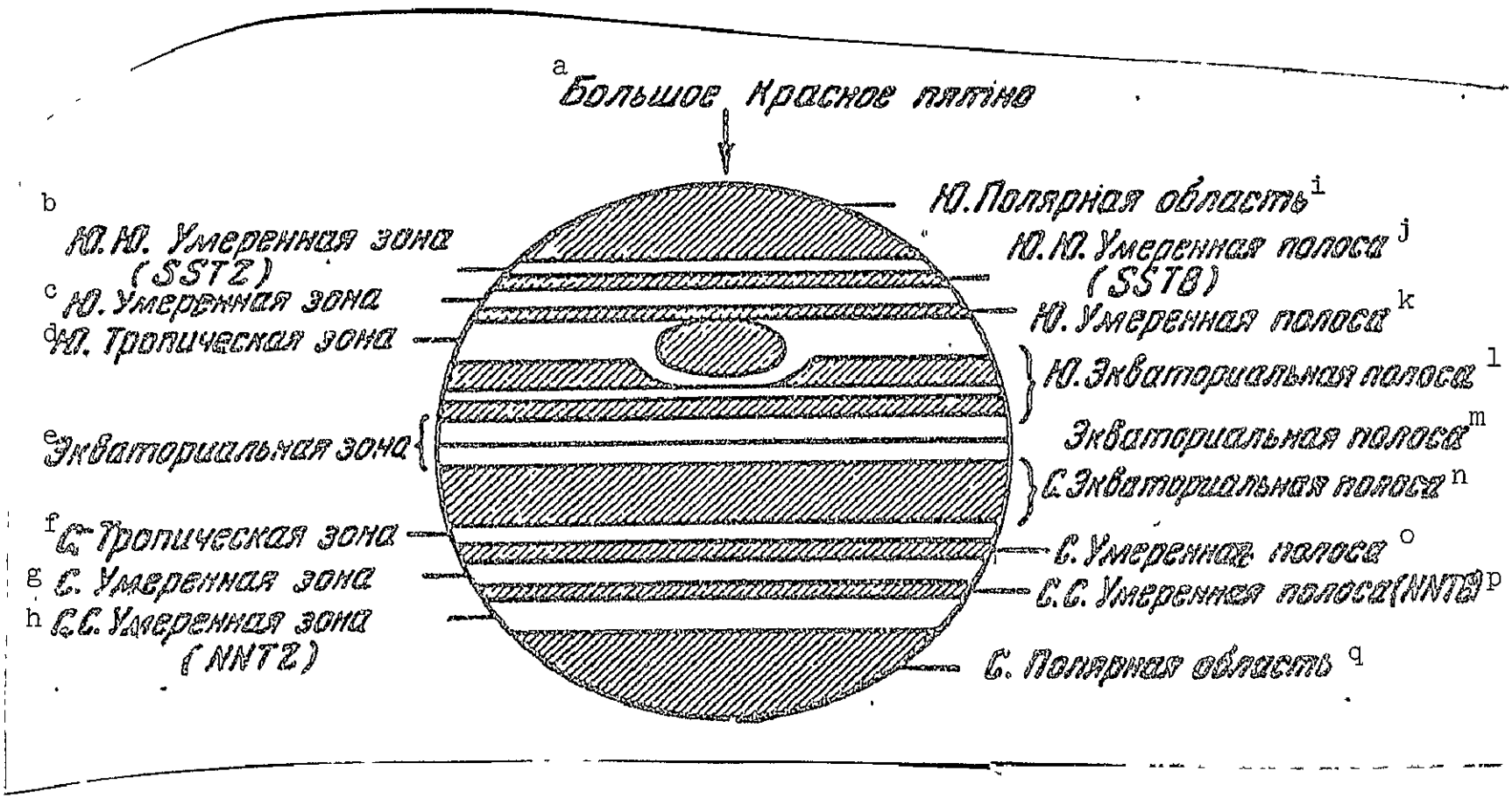

Fig. 5. Nomenclature of basic elements of horizontal cloud structure in atmosphere of Jupiter.

Key: a. Great Red Spot
b. S.S. Temperate Zone
c. S. Temperate Zone
d. S. Tropical Zone
e. Equatorial Zone
f. N. Tropical Zone
g. N. Temperate Zone
h. N.N. Temperate Zone
i. S. Polar Region
j. S.S. Temperate Band
k. S. Temperate Band
l. S. Equatorial Band
m. Equatorial Band
n. N. Equatorial Band
o. N. Temperate Band
p. N.N. Temperate Band
q. N. Polar Region

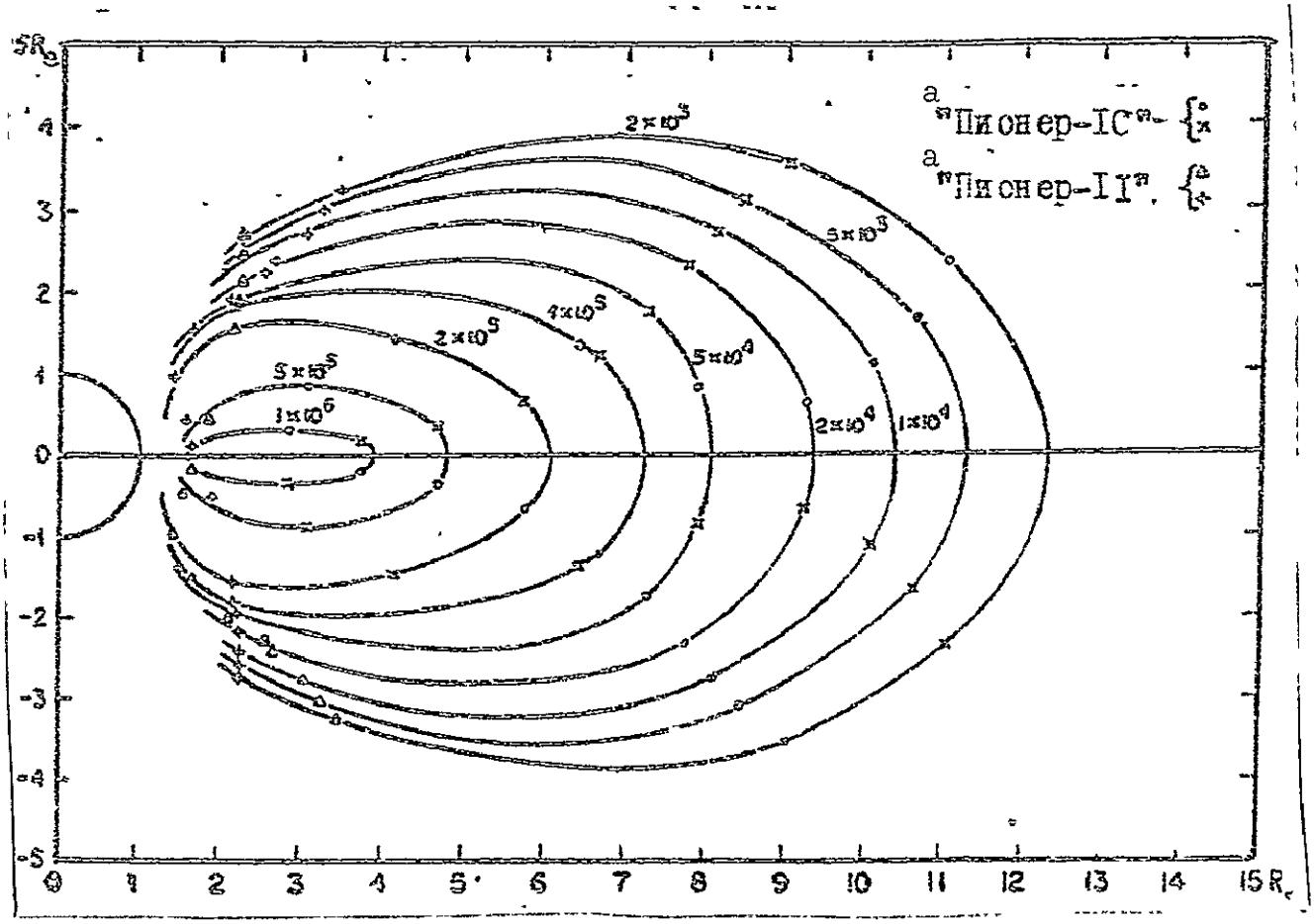

Fig. 6. Distribution of fluxes of electrons with energies E>21 MeV in stable radiation belt according to [55]; to obtain fluxes in particle·cm^{-2} units, reduced to isoline velocities, count in pulse·sec^{-1} must be multiplied by 23; ordinate, direction of magnetic field of planet; abscissa, magnetic equator.

Key: a. Pioneer

ORIGINAL PAGE IS
OF POOR QUALITY